Measurements of the Suitability of Large Rock Salt Formations for Radio Detection of High Energy Neutrinos

Peter Gorham[1], David Saltzberg[2], Allen Odian[3], Dawn Williams[2],
David Besson[4], George Frichter[5], & Sami Tantawi[3]
[1]*Jet Propulsion Laboratory, Calif. Institute of Technology, Pasadena, CA, 91109*
[2]*Department of Physics and Astronomy, University of California, Los Angeles, CA 90095*
[3]*Stanford Linear Accelerator Center, Stanford University, Stanford, CA 94309*
[4]*Dept. of Physics and Astronomy, University of Kansas, Lawrence, KS 66045*
[5]*Department of Physics, Florida State University*
(February 5, 2008)

We have investigated the possibility that large rock salt formations might be suitable as target masses for detection of neutrinos of energies about 10 PeV and above. In neutrino interactions at these energies, the secondary electromagnetic cascade produces a coherent radio pulse well above ambient thermal noise via the Askaryan effect. We describe measurements of radio-frequency attenuation lengths and ambient thermal noise in two salt formations. Measurements in the Waste Isolation Pilot Plant (WIPP), located in an evaporite salt bed in Carlsbad, NM yielded short attenuation lengths, 3–7 m over 150–300 MHz. However, measurements at United Salt's Hockley mine, located in a salt dome near Houston, Texas yielded attenuation lengths in excess of 250 m at similar frequencies. We have also analyzed early ground-penetrating radar data at Hockley mine and have found additional evidence for attenuation lengths in excess of several hundred meters at 440 MHz. We conclude that salt domes, which may individually contain several hundred cubic kilometer water-equivalent mass, provide attractive sites for next-generation high-energy neutrino detectors.

I. INTRODUCTION

The observation of several dozen single cosmic ray particles with energies beyond the $\sim 10^{19.5}$ eV Greisen-Zatsepin-Kuzmin (GZK) [1] cutoff poses among the most intriguing mysteries of high energy astrophysics. If our local region of the universe is not atypical, the detection of these particles implies a corresponding flux of 10^{17-19} eV neutrinos [2]. These neutrinos are secondary particles of the interactions of the super-GZK cosmic-rays, whose energy rapidly degrades over scales of a few tens of Mpc due to photomeson production on the 3K microwave background. [3] Detection of such neutrinos would provide unique information about the production and propagation of the particles near and above the GZK cutoff. This information is almost certainly necessary and in some cases sufficient to determine the nature of the primary cosmic rays and their sources. Characterization of these neutrinos is thus arguably of equal priority to the measurement of the super-GZK cosmic-ray spectrum.

Given standard estimates of the fluxes of the (presumably isotropic) GZK neutrinos [2], their detection will require of order several tens of cubic kilometers of water-equivalent instrumented mass with an acceptance solid angle of $\sim$ 1 sr, and at least several years of operation, assuming no background. A detector must also have reasonable calorimetric capability in order to establish the neutrino spectral signature of the GZK process. Present approaches, such as the water Cherenkov detectors AMANDA [4] and ANTARES [5], and the planned ICECUBE [6], are on a path which can achieve detection of these neutrinos through muon tracking techniques and detection of high energy cascades. The RICE project [7–9], utilizing cascade radio emission to search for such interactions, provides an alternative radio-Cherenkov detection method, also in Antarctic ice, as part of the AMANDA project. Both the optical and radio approaches will require significantly larger volumes to approach sensitivity to GZK neutrinos. Here we describe measurements which indicate the viability of an alternative medium to ice, that of subterranean natural salt formations, which are abundant throughout the world. As we will show here, salt formations exist with dielectric properties that are competitive with polar sheet ice, and these may thus provide a cost-effective approach to the challenging problem of GZK neutrino detection.

The first suggestion that naturally occurring rock salt formations could be a viable neutrino detection medium can be traced back to G. A. Askaryan [10], who first proposed the coherent Cherenkov mechanism for radio pulse production by charge asymmetry in electromagnetic cascades. The asymmetry arises from photon and electron scattering processes on the surrounding medium and from positron annihilation in flight, and leads to a net $\sim 20\%$ excess of electrons over positrons in the shower. Askaryan's effect was revisited with detailed simulations in the 1990's [11–13] has recently been confirmed in accelerator measurements at Argonne and SLAC [14,15].

The resulting coherent radio emission, the power of which rises quadratically with shower energy, dominates all secondary radiation processes (for example, optical Cherenkov) in electromagnetic showers above about 10 PeV. With remarkable prescience, Askaryan noted that, if there were neutrinos above these high energies, clear natural dielectric media such as rock salt, ice, or even the lunar regolith, might provide the necessary large volumes needed for a suitable neutrino target.

Spurred on by a revival of interest in techniques for radio detection of cascades [16], and by some recent efforts in laboratory measurements of natural salt samples [17], we have made *in situ* measurements of the dielectric properties or rock salt in two underground salt excavations: the Waste Isolation Pilot Plant (WIPP) in New Mexico, and the United Salt Corporation's Hockley mine, within the Hockley salt dome near Houston, Texas. In the following section we provide some background material on these sites and measurements of their dielectric properties. We then report on the two sets of experiments conducted and their results. Section 5 presents a reanalysis of some earlier unpublished data from ground-penetrating radar measurements in the Hockley mine. In section 6 we discuss the implications of our results, and our conclusions.

II. GEOLOGICAL & DIELECTRIC PROPERTIES OF SALT FORMATIONS

A. Geological properties

Rock salt deposits are distributed throughout the world and occur primarily in the form of 1) bedded salts and other minerals (known as *evaporites*) consisting of layers of dried solutes from ancient oceans; and 2) evolved salt structures which are thought to form from the deformation of deeply bedded salt through tectonic and buoyant forces. The latter type includes the so-called *salt diapirs*: formations such as salt domes and salt walls which involve apparent extrusion of large masses of bedded salt into overlying rock. This extrusion process is thought to be driven by the fact that rock salt is generally less dense ($\rho = 2.2$ g cm^{-3}) than most other rocks, and at the high temperatures of the salt beds at depths of 10 km or more, the salt plasticity increases [18,19].

During the process of diapirism, through a sequence of events which is not well understood, the impurities in the salt tend to segregate away from the main salt body, and the salt tends to become more pure than the initial bed from which it arises. In general, where bedded salt may contain significant entrapped brine and numerous mineral impurities, salt domes tend to produce salt with negligible brine content and minimal impurities. The most common residual impurity in salt domes is anhydrite ($CaSO_4$), which occurs at the 1–5% level in many domes.

B. Dielectric properties

1. Pure salt

Pure crystalline NaCl (the mineral *halite*) is known to have extremely low loss for propagation of radio waves from frequencies of a few MHz up to 10 GHz and more. Because of the simple ionic structure of the NaCl crystal, there are no first-order ionic or vibrational modes that can absorb energy in this frequency range, and any absorption or scattering that does occur is due primarily to activation of lattice defects [20]. Radio-frequency (RF) absorption in dielectrics is usually described in terms of the loss tangent. For low-loss materials the loss tangent is approximately the tangent of the change in phase angle of the electric and magnetic fields of an electromagnetic wave with respect to a lossless medium. It is given simply by

$$\tan\delta \;=\; \frac{\epsilon''}{\epsilon'} \tag{1}$$

where ϵ'', ϵ' are the imaginary and real parts of the relative dielectric permittivity.

The loss tangent is related to field attenuation coefficient α (the inverse of the distance over which the electromagnetic field strength falls to $1/e$ of its value) by [21]:

$$\tan\delta = \left(\left[\frac{2}{\epsilon'}\left(\frac{\alpha c}{2\pi\nu}\right)^2 + 1\right]^2 - 1\right)^{1/2} \tag{2}$$

where c is the speed of light and ν the radio frequency. Conversely, the field attenuation length L_α is given by

$$L_\alpha \;=\; \frac{1}{\alpha} = \frac{\lambda_0}{2\pi}\left[\frac{2}{\epsilon'(\sqrt{1+\tan^2\delta}\;-1)}\right]^{1/2} \tag{3}$$

where λ_0 is the free-space wavelength of the radiation. For the low-loss media ($\epsilon''/\epsilon' \ll 1$) considered here, the relationship is well approximated by

$$L_\alpha \approx \frac{\lambda_0}{\pi\sqrt{\epsilon'}\tan\delta}. \tag{4}$$

For pure crystalline NaCl, $\epsilon' = 6.0$ and $\tan\delta \leq 10^{-4}$ over the frequency range from ~ 1 MHz to several GHz, and the implied attenuation length at $\lambda_0 = 1$ m (300 MHz) is $L_\alpha \geq 1.3$ km.

2. Naturally occurring rock salt

As noted above, the purity and thus the dielectric properties of natural salt deposits vary widely. Salt found in bedded evaporite deposits in North America shows dielectric constants ranging from 5-7 and loss tangents from 0.015–0.030 or more at 300 MHz [22], implying attenuation lengths below 10 m, although more transparent evaporite salt may be found occasionally in some layers.

In salt domes and other diapirs, the situation changes dramatically. During the late 1960's and early 1970's, there was a significant effort on the part of mining geologists to develop ground-penetrating radar (GPR) techniques that could provide for "look-ahead" capabilities in tunnel mining, to mitigate risk. Thus numerous measurements of salt dome transparency using GPR techniques are available in the geology literature, although the transparency results are seldom expressed directly in terms of the loss tangent. Unterberger [23] and Stewart & Unterberger [24] report VHF loss tangents of 10^{-4} for samples of several Gulf Coast salt dome halites, and in some cases they measured values as low as 2×10^{-5}. Measurements of the attenuation length *in situ* are not common, however. Typically GPR reports detail the returned power of reflective regions within the salt mass, often at great distances. In several cases, the radar systems were able to detect reflections from the flank of a salt dome up to 1.5 km distant, with relatively low power radar systems (typically a few watts peak transmitted power) [24].

Several conclusions can be gleaned from the GPR measurements of salt domes. First, RF propagation through the salt is relatively free from significant bulk scattering effects. If the scattering length were short compared to the two-way propagation distance in many of these experiments, the short pulses used in the radar system (in some cases less than 10 ns) would not remain coherent. This is not to say that there are no inhomogeneities in the salt mass that can scatter radiation; these are certainly present, but tend to be discrete and widely spaced.

Second, there appear to be no significant depolarization effects in RF propagation through the salt. Since most transmitters used 100% polarized radiation (either linear or circular) and received also one polarization, the coherence of specular reflections received in two way trips of several km could not be retained if there were any depolarization or even polarization rotation, such as through birefringence.

Finally, there is no evidence for any significant dispersive effects in low-loss salt over the frequency range from 100-1000 MHz. This can be concluded from comparison of the

dielectric constants for many different measurements at many different frequencies in this range; all find values very close to that of pure salt.

III. WIPP EXPERIMENTS

The Waste Isolation Pilot Plant is primarily a repository for nuclear waste, but has also been directed to support underground experimental research. If the WIPP halite were found to have favorable properties for RF transmission, then significant infrastructure would be available to support development of a large neutrino detector. The WIPP facility is operated almost exclusively on a single *horizon* (or horizontal level) at 655 m depth below the local surface. The tunnels, known as *drifts*, are typically between 7–15 m wide and about 5–6 m high. The average WIPP halite is 90–95% pure, the remainder consisting of clay, anhydrite, polyhalite, and trases of saturated brine. The disposal horizon is located in the 2000 feet-thick Salado salt near Carlsbad, New Mexico. That salt sequence, which is more than 250 million years old, is part of a series of sedimentary rocks filling the Permian Basin, which extends over portions of Kansas, Texas, Oklahoma and Colorado.

Some prior measurements of the dielectric properties of four samples of Carlsbad halite cored from a 755 m depth are given by Olhoeft [26] up to a frequency of 1 MHz. At this frequency he found $\epsilon' = 7.0 - 8.7$ and $\tan\delta = 0.22 - 0.36$. GPR measurements at WIPP have also been recently done [27] at 500 MHz, however no estimates of the attenuation length of loss tangent were reported. The goal of the GPR was to perform high-resolution mapping of features close to the drift walls, thus no targets deeper than ~ 5 m were reported. Roggenthen [28] did report that transmission through approximately 30 m of salt was also achieved through one or more columns but no estimates of the transmitted power or receiver dynamic range were available.

We report here on radio attenuation length measurements made in December 2000. Our principle measurements are derived from three four inch diameter bore holes, separated by 22.86 m along the ceiling centerline of room-6, Panel 2, 655 m below the surface. Each hole extended 6.71 m above the ceiling. Balanced copper dipole antennas (length=27 cm, diam.=2.5 cm) were raised into the holes using 1/2" rigid heliax cable at a nominal height of 5.49 m above the ceiling corresponding to the center of the purest accessible halite layer. Note that the ceiling and floor of the drifts follow the geological strata so that the antennas at the same height above the ceiling are in the same layer. The signal pulse used for these and the following measurements in the Hockley mine consisted of a 10-100 ns pulse, modulated with frequencies from 90-500 MHz.

The signal was sent to a dipole in one of the boreholes which transmitted into the halite. The signal was received by a dipole inserted into another of the boreholes, then amplified by two cascaded, but physically separated, broadband amplifiers for a total gain of ~ 57 dB. The output of the second amplifier was filtered by an appropriate bandpass filter about the center frequency to improve the signal/noise ratio. The received signal was recorded by a digital oscilloscope. When the transmitting dipole was moved from the end to center hole, the acquisition system (amplifiers, cables, filters etc.) were kept identical so that the overall system gain did not need to be known.

The field attenuation factor, α is determined from the received voltages, V_1 and V_2 at two distances, d_1 and d_2 by,

$$\frac{V_2}{V_1}\frac{d_2}{d_1} = \exp(-\alpha(d_2 - d_1)). \tag{5}$$

Attenuation lengths vs. frequency at this stratum are summarized in fig. 1. Only signals between 110 and 175 MHz coupled well enough to be easily observed at the far hole. At 300 MHz, the pulse was extracted from the noise using a cross-correlation with the transmitted pulse shape. The assigned uncertainties are due to a 15% r.m.s. azimuthal asymmetry of the dipoles and 0.5 m distance uncertainty. The data are fairly well described by a loss-tangent that is independent of frequency. We do, however, see some evidence for a slow decrease in loss tangent versus frequency as would be consistent with the presence of some brine at these frequencies [21] so we fit the data to a frequency-dependent loss-tangent:

$$\tan\delta(\nu) = a + b\frac{\nu - \nu_0}{\nu_0}, \tag{6}$$

where a would be the loss-tangent if it were frequency independent and b is a small correction. We chose $\nu_0 = 200$ MHz in the parameterization to minimize the correlation between a and b. The lower set of data in fig. 1, which includes a 300 MHz point, fits to: $a = 0.0627 \pm 0.0031$ and $b = -0.020 \pm 0.008$ In the upper set of data, which did not include a 300 MHz point, a and b were highly correlated but we find $a = 0.0343 \pm 0.0036$ and $b = -0.019 \pm 0.012$. Both sets are thus consistent with perhaps a slow decrease of loss tangent at increasing frequency, as expected from the behavior of the loss tangent of brine.

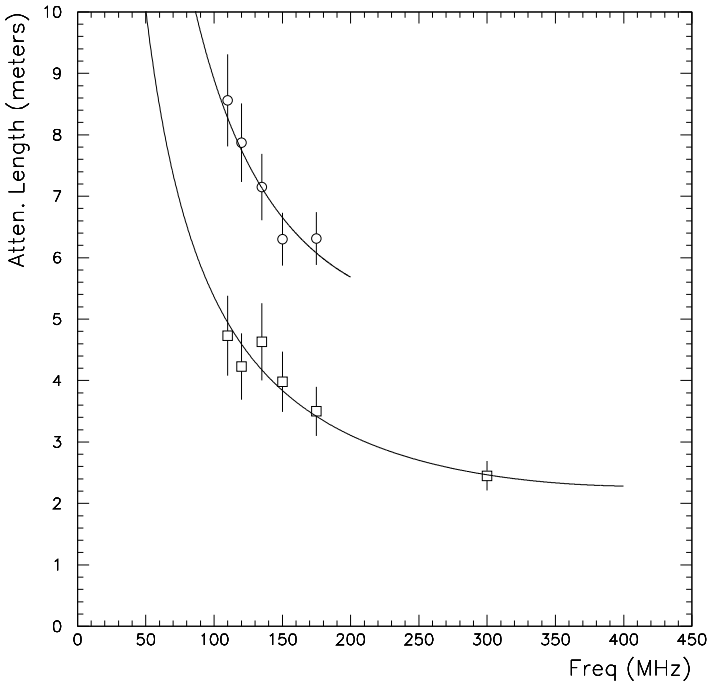

FIG. 1. Measured field attenuation length versus frequency from the two sets of three holes.

We anticipated that the attenuation length would depend on geological layer since the relative amounts of impurities, clay and anhydrite, vary significantly. Measurements vs. height were made at 150 MHz, where the antenna coupling was observed to be the most efficient. The attenuation length measurements were made between only two boreholes and are normalized to the value measured at 5.5 m. The results are summarized in Table I. Despite the changes in attenuation length, less than 0.5% variation in the index of refraction for the various layers was observed.

The delay of the 150 MHz pulse train over 23 m vs. 45 m gave the index of refraction to be 2.82 ± 0.03. This may be compared with the measured value for pure salt, 2.45. Since both anhydrite and clay have lower indices of refraction than halite, the difference may be due to moisture known to be trapped in the clay-rich layers of the salt. Water has an index of refraction of about 9 at these frequencies and a very high loss tangent, so its presence may be the cause of both the short attenuation length and the anomalously high index of refraction.

TABLE I. Attenuation length versus stratum as measured in height of antenna above ceiling. These measurements are normalized to the value measured at 5.5 m. Uncertainties are systematic as described in the text.

height above ceiling (meters)	impurity present	attenuation length (meters)
3.7	clay	3.4 ± 0.5
4.6	anhydrite stringers	4.1 ± 0.6
5.0	anhydrite stringers	6.3 ± 0.9
5.5	least anhydrite	$\equiv 6.3$
5.9	some anhydrite	3.6 ± 0.5
6.4	some anhydrite	4.5 ± 0.7
6.7	much clay/some anhydrite	4.2 ± 0.6

IV. HOCKLEY MINE EXPERIMENTS

The Hockley salt dome was discovered in 1905 due to gas seeps and other evidence for trapped oil reservoirs in the area. Some oil production has continued up to recent times but the dome is not highly productive for oil. In 1930 the Houston Salt Company drilled a shaft in the northeast part of the dome and began mining salt at a depth of 460 m in 1934, but ceased operation within several years. The United Salt Company acquired the mine in 1946 and has continued to mine salt until the present [30]. The current mine covers an area of several square km in a grid of 10-15 m wide by 5-8 m high drifts, and rectangular columns typically 30 m by 40 m in cross section.

The top of the salt structure begins at a depth of about 300 m below the local surface. The dome is roughly elliptical in horizontal cross section, with major and minor diameters of 3.6 km by 2.9 km at the mine level. The cross section of the dome continues to grow with depth to at least 2 km, where it is 4.4 km by 3.3 km. The salt structure itself is thought to extend down to 10 km depth, with an inverted teardrop shape that narrows at the base. The estimated volume of salt in the dome is of order 80 km^3 [31], with of order 20-25 km^3 contained within the top 3 km of the dome. [19]

We made measurements in the Hockley mine in June 2001. For the Hockley mine experiments, boreholes were not available, and measurements were made primarily with two antennas: a half-wave dipole that was tuned to peak at 150 MHz in salt, and which worked also at the full-wave resonance at 300 MHz. This antenna was found to behave reasonably well if it were in contact with the salt surface, although we could not measure the modified beam pattern of the antenna. We also made use of a UHF 4-bay bowtie antenna with a ground-plane and approximately 12 dBi of gain for measurements where the antenna was aimed into the salt from an external position. This latter antenna was used primarily at a frequency of 750 MHz.

In all cases, our goal was to was to make measurements over several different distances with the same antenna and cable configuration, so that we could make use of relative measurements which would not require absolute antenna calibration. Our ability to do this was constrained by the geometry of the region of the mine where we were able to operate, and we found in several cases that the local shape of the wall and other anomalies prevented our using some of the positions.

Figure 2 shows a layout of the region of the mine where we made our measurements. The grid is in mine coordinates which are $100'$ squares aligned along compass directions. The primary positions of the receive antenna are indicated by the letters A,B,C. Most of the measurements were made with the transmitting antenna along either the north or west walls as indicated. However, we also made some tests using the longer distance to the east, between positions C & D (about 40 m) and C & F (about 90 m). In these latter cases the mine drift was at a 4–6 m lower elevation than the receive antenna, and some difficulties were encountered with questionable emplacement of the antenna, due to the presence of fractures in the salt wall of the drift. Thus although we were able to successfully transmit through the salt at both 150 MHZ and 300 MHz at these locations, the data were not repeatable enough to give reliable results.

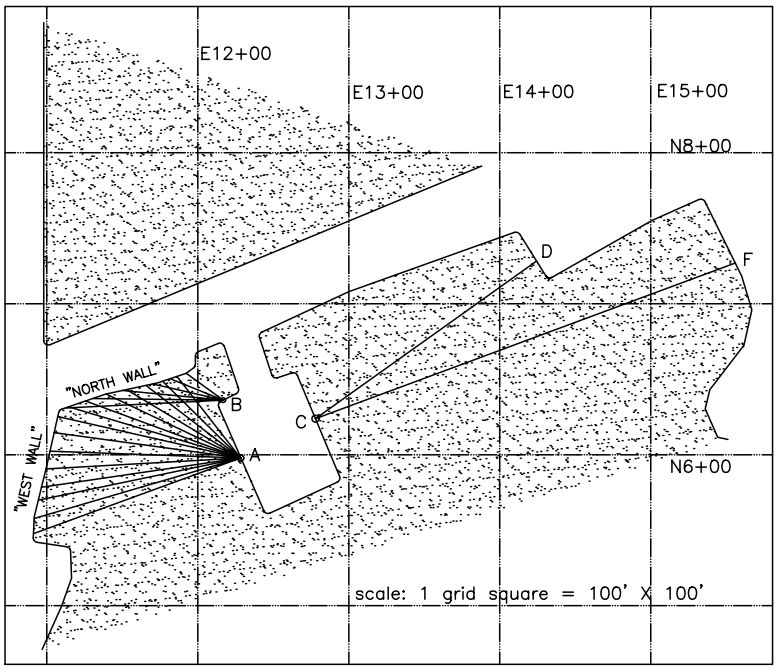

FIG. 2. Layout of the region of the mine where our Hockley measurements were made. Typical rays for the measurements are shown.

One of the recurring difficulties was due to the fact that while obtaining a range of distances for the measurements, we could not retain normal-incidence angles for the transmission or reception antennas. For vertical dipole measurements, the beam pattern has nominal azimuthal symmetry. However, the presence of the salt-air interface modifies this pattern significantly, particularly for rays that are far from normal incidence.

A. Attenuation measurements

1. Absolute field strength measurements.

As can be seen from Fig. 2, a large number of measurements were made along both the north and west walls, with distances ranging from about 12 to 45 m. To obtain an indication of whether there were any overall gross systematics in the transmission or receiving of the signals, we here perform an analytical estimate of the expected received signal compared to the pulse which was measured on transmission. Although we found large scatter in the measured data, this procedure will provide a first-order evaluation of the attenuation in the salt and will indicate whether there is a subset of higher quality measurements that can be reasonably used to improve this estimate.

The Friis formula for the relationship between transmitted (T_x) and received (R_x) power in an antenna is given by

$$\frac{P_{R_x}}{P_{T_x}} = \frac{A_{T_x} A_{R_x}}{\lambda^2 R^2}, \tag{7}$$

where A is the effective area of the transmitting or receiving antenna, λ is the wavelength in salt and R is the distance between the two antennas.

Recasting this equation in terms of the voltage measured:

$$\frac{V_{R_x}}{V_{T_x}} = \sqrt{\frac{A_{T_x} A_{R_x}}{\lambda^2 R^2}}. \tag{8}$$

Noting that $A_{T_x} = A_{R_x}$, we have

$$\frac{V_{R_x}}{V_{T_x}} R = \frac{A}{\lambda}. \tag{9}$$

The effective areas of a half-wave dipole and full-wave dipoles are $0.13\lambda^2$ and $0.048\lambda^2$, respectively. [32] The dipoles used at Hockley are half-wave at 150 MHz and full wave at 300 MHz, so at 150 MHz,

$$\frac{V_{R_x}}{V_{T_x}} R = 0.13\lambda, \tag{10}$$

while at 300 MHz,

$$\frac{V_{R_x}}{V_{T_x}} R = 0.048\lambda. \tag{11}$$

Figure 3 shows the quantity $\frac{V_{R_x}}{V_{T_x}} R$ plotted for all of the data at 150 and 300 MHz. The dashed line shows the absolute value for $\frac{V_{R_x}}{V_{T_x}} R$ given by the Friis formula. The data were taken in six distinct "runs" with one of the dipoles kept in a fixed position and the other dipole was moved. The runs with the least repeatability were taken with the fixed dipole near a large irregularity in the surface of the wall. The data points are corrected for cable attenuation, amplifier gain, and for reflection losses. At 150 MHz, ∼30% of the power sent to the transmitting antenna is reflected back. At 300 MHz, the reflected power was not directly measured, so the same reflected power is assumed for 300 MHz. Note that the Friis formula assumes a dipole pattern, which is not completely accurate in our case since the antenna pattern was half in salt and half in air. We have made no correction for this effect.

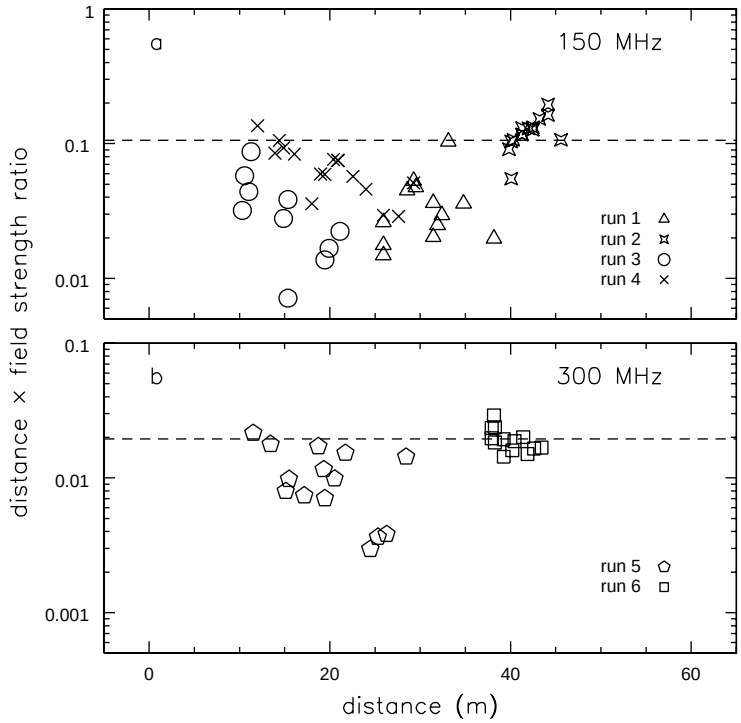

FIG. 3. Field strength measurements for all of the data taken along the N and W walls at (a) 150 & (b) 300 MHz. The dashed line is the expected value without attenuation.

The data points are consistent, within an order of magnitude, with the value given by the Friis formula, which assumes no attenuation due to the medium. Note that the points at the farthest distance were taken with the best geometry and showed the least scatter. By virtue of having the greatest separation, these data also have the best sensitivity to attenuation losses. These samples show no measurable attenuation. Therefore the data are consistent with a very long attenuation length, well in excess of 40 meters.

2. Relative field strength measurements.

To improve the precision of our estimate of the attenuation length, we have excluded runs 1 and 3 of the 150 MHz data due to questions about coupling systematics, and we have excluded the top and bottom 10% outlying samples of the remaining data. We have grouped the data in appropriate range bins and averaged the received pulse power for each range bin. No correction has been made for non-normal incidence angles. After averaging we then convert back to the mean field strength by taking the square root of the result. The fractional power variance of the averaged data provides an estimate of the precision of the field measurement.

As noted above, in the far field the ratio of the received (R_x) to transmitted (T_x) voltage in an antenna should behave as

$$\frac{V_{Rx}}{V_{Tx}} = \frac{\kappa}{d}\exp(-\alpha d) \tag{12}$$

where d is the distance between the transmitting and receiving antennas, α is the field attenuation coefficient, and κ is an unknown constant scale factor which accounts for the system losses. In Fig. 4(a) and (b) we plot $(V_{Rx}/V_{Tx}) \times d$ on a logarithmic scale as a function of distance for 150 and 300 MHz, where we have now normalized to the mean power. The plot also shows the results of fits to the exponential attenuation factor (here expressed in terms of its inverse, the attenuation length). Note that the error bars from the exponential fit are markedly asymmetric and that values below zero for either attenuation coefficient or attenuation length are unphysical. The uncertainties are given as the range of the 67% confidence interval. Thus, for Fig. 4(a), the 150 MHz attenuation length is consistent with 34 m at the low edge of the confidence interval, but is inconsistent with values below 20 m at the $\geq 95\%$ confidence level.

3. Attenuation ratio for 300 to 150 MHz.

Because the 300 MHz and 150 MHz measurements were made with the same antenna used in full- and half-wave dipole mode, a relatively simple relationship holds between the attenuation measurements for the two frequencies. If the loss tangent is nearly constant with frequency, which we expect from our previous measurements at WIPP, then the field attenuation coefficient is proportional to the frequency. That is, the attenuation length at 300 MHz is half of the attenuation length at 150 MHz. Then

$$\frac{V_{Rx^{300}}}{V_{Tx^{300}}} \left[\frac{V_{Rx^{150}}}{V_{Tx^{150}}}\right]^{-1} = \exp(-\alpha_{150}\ d)\ . \tag{13}$$

Thus by taking the ratio of the two relative attenuation measurements, we obtain a partially independent measure of the attenuation at 150 MHz, under the assumption of a constant loss tangent. Note that we found a slight deviation from a constant loss tangent at WIPP. We attribute that deviation to the brine and other impurities trapped in the salt at WIPP that is not present at Hockley. Measurements of Texas salt dome halite in the early 1970's [29] do report a slow decrease of the loss tangent with frequency for low-loss salt. If we chose to apply a correction for this effect to these data, it would have a small effect ($\sim$20%) on the reported attenuation length derived from this ratio. Figure 4c shows this ratio on a logarithmic scale as a function of distance. For these data, the slope of the logarithm is a measure of the attenuation length as described above. A fit of the data to a falling exponential indicates a large value for the attenuation length; however the fitted uncertainties are also large, and the result is consistent with the previous results. It is evident that a 150 MHz attenuation length much greater than 40 m is favored by the data.

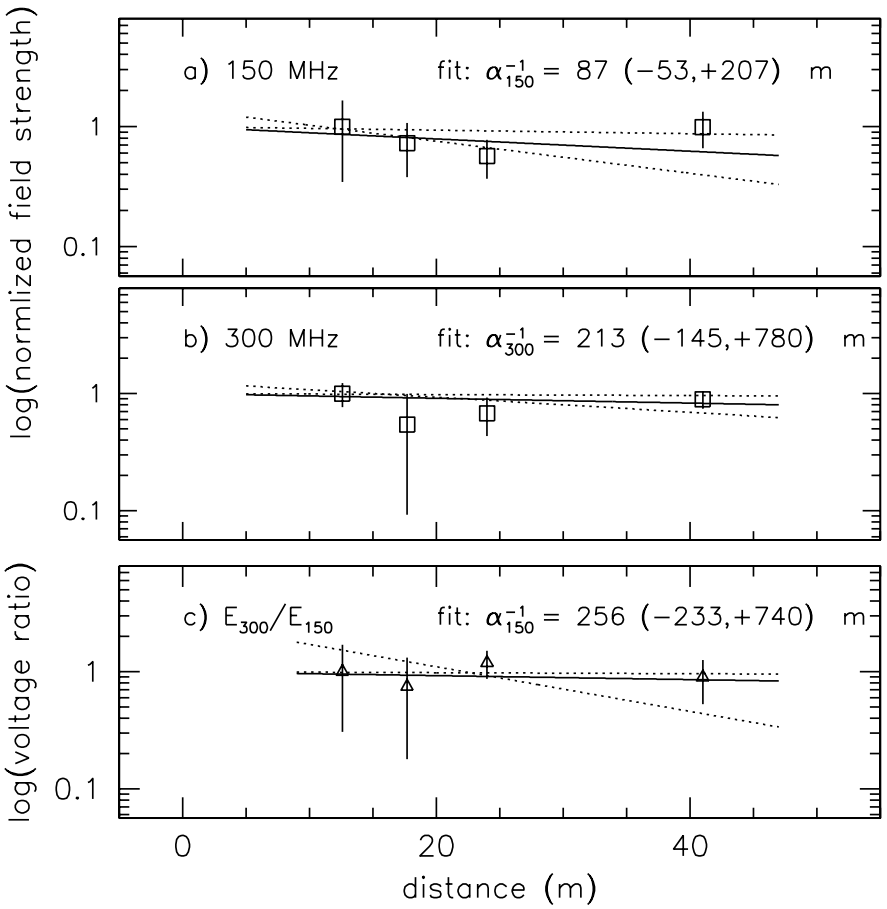

FIG. 4. Plots of binned field attenuation measurements. (a) The data at 150 MHz, with exponential fit shown as a solid line, including 67% confidence interval in dotted lines. (b) Same as (a) for 300 MHz. (c) Ratio of (b) over (a), which gives a partially independent estimate of the 150 MHz attenuation length, shown as a fitted line as in (a) and (b).

4. Attenuation at 750 MHz.

We also made measurements of transmission at 750 MHz using a commercial UHF antenna consisting of four phased bowtie antennas. Because this antenna array had a much narrower beam than the dipoles we used, we were affected more by the difficulty of alignment of the antenna beam for the transmit and receive antennas. Because of wide variations in the received power, we chose in this case to only use only the highest $\sim 50\%$ of the measured values to reduce the otherwise significant scatter. (This was only done for the 750 MHz data which were taken with a high gain antenna.) This approach is in general justified since beam misalignments and coupling problems produce only losses and lensing effects can be neglected here [33]). The data were then power averaged within appropriate range bins. In this case, we have combined data from two separate runs which are offset by an unknown normalization, by rescaling each data set to its mean power.

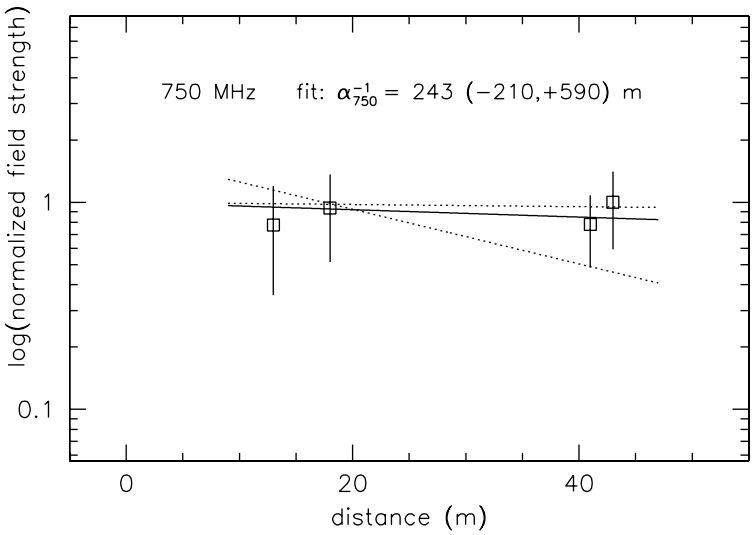

FIG. 5. Similar to previous figure, for 750 MHz data.

The results of the 750 MHz analysis are shown in Fig. 5. Again there is little or no evidence for attenuation, and the fitted value shown is not strongly constrained by the data. It is remarkable that despite the factor of 2.5 increase in frequency from 300 MHz, the data are still consistent with an extremely long attenuation length.

B. Polarization measurements.

A half-wave dipole, which produces linearly polarized radiation with electric field vector aligned with the dipole axis, typically provides about 20 dB of cross-polarization rejection. We made measurements at 150 MHz of the cross-polarization leakage through a distance of 45 m of the salt. The net cross-polarized power observed was $(1.55 \pm 0.1)\%$ of the co-polarized power. This is consistent with no polarization leakage since this is within the cross-polarized rejection limits of the antennas.

We note that this measurement also indicates a lack of significant birefringence of the salt, since any rotation of the plane of polarization would appear as a noticeable cross-polarization leakage. Using the same cross-polarized power above, the implied limit on the rotation angle Ψ of the plane of polarization is $\Delta\Psi \leq (0.16 \pm 0.01)^\circ$ m^{-1}. Thus the phase difference between two circularly polarized modes will not exceed 1 radian in 360 m of propagation distance in the salt.

C. Noise environment

The overburden of rock above the salt dome should insulate the environment well from terrestrial radio-frequency interference (RFI). We measured the noise environment at the Hockley site using the same short dipole used at 150 MHz. We calculated that the system temperature of our apparatus was 770 K including front-end amplifier noise (263 K) , cables (1.2 dB at 310 K), and 310 K salt filling the antenna aperture. We observed no departure from uniform power in the power spectrum. We could not observe any difference between observing the salt through an antenna versus a 50 Ω load at the front-end amplifier input. We could have detected excess power from the salt (above its blackbody temperature) of order 100 K if it were present. Hence we conclude the noise environment may be characterized as fluctuations of a 310 K blackbody spectrum. On rare occasions we could see clear RFI due to the use of walkie-talkies by local mining crews. Such events in a salt detector would be easily removed by offline analysis but could cause a high trigger rate. To keep the trigger rate low, a salt detector in the mine might require tuned notch filters for the communication frequencies in use at the facility.

V. ANALYSIS OF UNPUBLISHED GPR DATA FROM HOCKLEY

As we have noted earlier, there is a significant body of geophysics literature on ground-penetrating radar measurements of salt formations. In particular, J. Hluchanek, under the supervision of R. Unterberger, completed a master's thesis using GPR measurements in the Hockley mine [30]. In this section we analyze some of these results with the goal of obtaining an independent estimate of the attenuation length.

The Texas A&M GPR system used a beamed Yagi-Uda antenna at 440 MHz. Since the primary goal of these measurements was to establish the utility of GPR for forward-looking assessment of the path of a mined tunnel, almost all of the data consist of measurements of the amplitudes of reflections from inhomogeneities within the salt, at several positions within the mine, and at various distances within the salt mass, ranging from about 50 m to over 350 m from the transmitter. Having measured the salt index of refraction (2.45 ± 0.05, consistent with pure salt), Hluchanek was able to establish the target distances to a precision of several m, and estimate the received power over a dynamic range of about 50 dB. No absolute measurements of the transmitted or received power were given, except that the transmitter itself operated at about 3 W peak power.

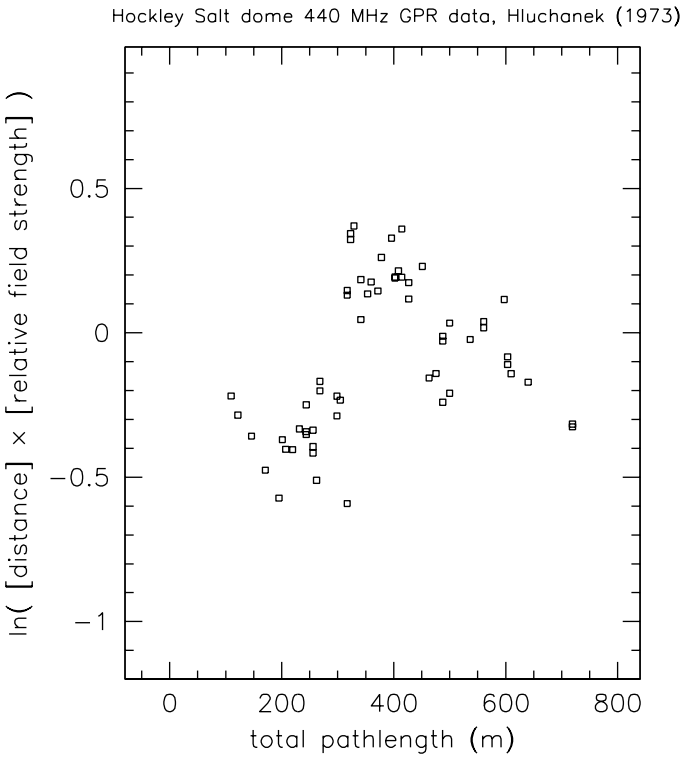

FIG. 6. Measurements of relative received field strength from radar targets in the Hockley mine. The data have been boxcar smoothed with over ±5 adjacent data points to reduce the variance.

Given these data, we arrive at a first order estimate of the attenuation length by assuming that the ensemble of reflective inhomogeneities has a well-defined mean reflectivity with a quasi-normal distribution around this mean. Since, when a target was seen in the radar return, the antenna was then adjusted to maximize the return power, we can in general ignore the antenna beam effects. Hluchanek also made Snell's law corrections for cases of non-normal incidence in the geometry.

Figure 6 shows a plot of the field strength data, multiplied by the two-way propagation distance to remove the radial loss factor. Here we have smoothed the power measurements with a 5-sample boxcar average to reduce the scatter, and then converted to field strength by taking the square root. It is evident that the data do not follow a simple exponential as would be the case for a uniform reflectivity of the targets. A simple fit to all of the data in this case would yield no measurable attenuation. However we can calculate an attenuation length by fitting only targets at distances above 300 m, treating them as a uniform ensemble. This approach is somewhat more conservative than fitting the entire data set, since the data below 300 m would tend to force a much longer attenuation length.

Fig. 7 shows the results of this approach. Now we have binned the data in 75 m bins, with uncertainties assigned according to an estimate of the power-weighted variance of the data in each bin. The resulting fit is plotted as in the previous section. The uncertainties shown are only statistical; clearly there are several possible systematic uncertainties that could impact this analysis. However, the indications are again that the attenuation length in the VHF to UHF regime in the Hockley dome is of order several hundred meters at least. Such long attenuation lengths are in fact quite difficult to accurately measure under any

conditions, whether in the laboratory or *in situ*.

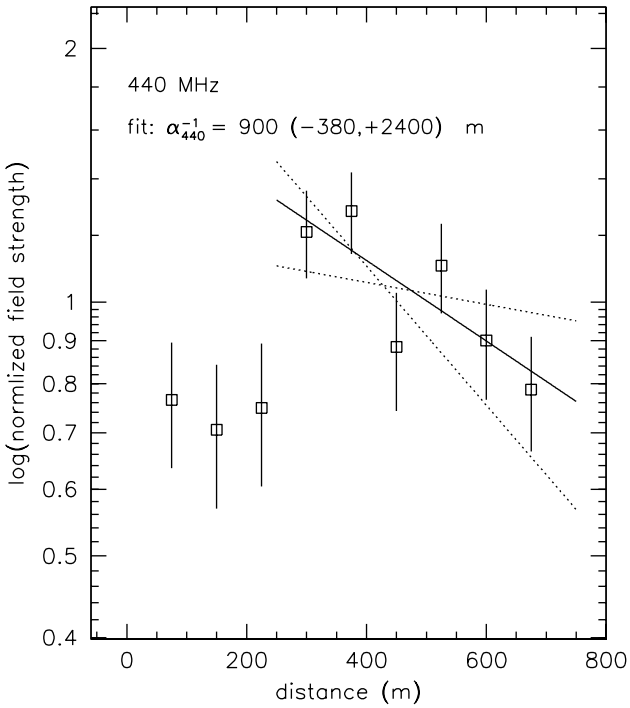

FIG. 7. A plot of the GPR data, now binned in 75 m bins. The fitted lines are the fit of only the data above 300 m, and the 67% confidence interval fitted lines are also shown. Quoted uncertainties are statistical only, and do not include potentially significant systematic errors.

VI. DISCUSSION

We have established that naturally occurring salt formations exist with extremely long radio attenuation lengths, comparable or better than the clarity of pure water or ice at optical wavelengths. We should note here that we have followed the RF convention [21] and expressed attenuation lengths in terms of the field attenuation rather than power or intensity attenuation, as is more common at optical wavelengths. However, using the separate definitions is appropriate for comparing techniques, since at radio frequencies the detection is coherent and signal strength increases linearly with field strength. In optical detection of Cherenkov radiation, the fields sum incoherently, and the signal strength increases linearly with intensity rather than field strength.

A natural dielectric material that has RF attenuation lengths comparable to that of salt is clear glacial or polar shelf ice. As we have noted in the introduction, the RICE experiment has already begun to exploit this property of ice in the search for neutrino interactions [7–9]. It is thus of interest to compare and contrast the properties of ice and salt for this purpose.

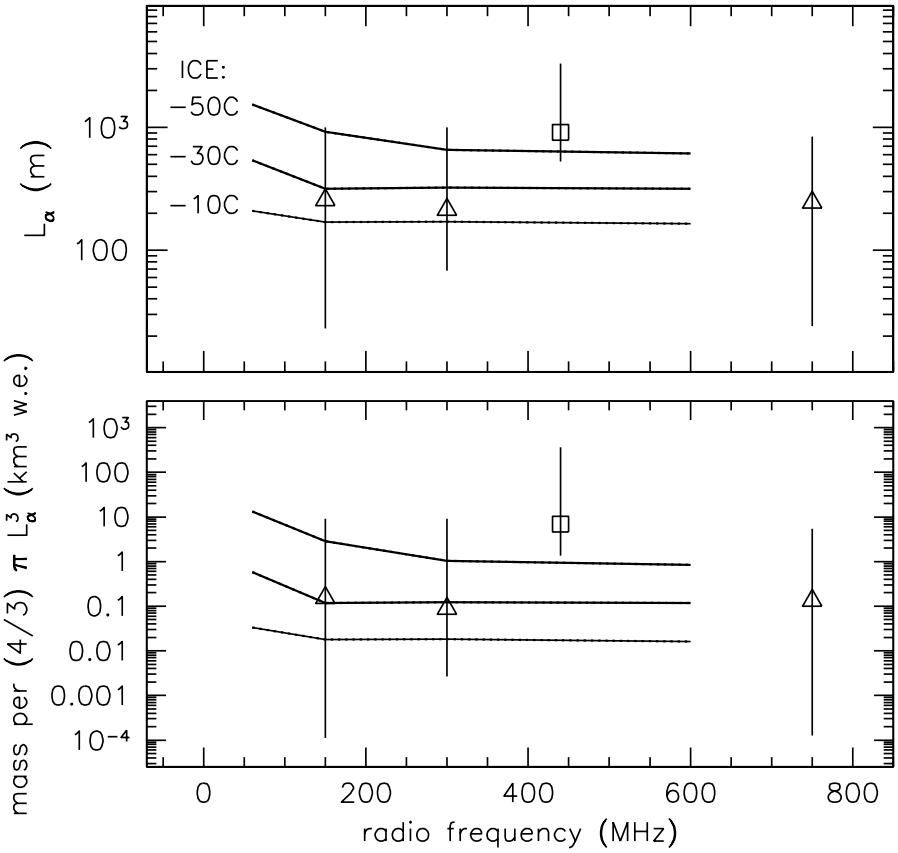

FIG. 8. Top: Attenuation lengths of antarctic ice for various temperatures, and for the salt results reported here. Bottom, enclosed mass (in water-equivalent cubic km) within one attenuation length radius for ice and salt. Triangles are the data taken by our group; squares are the re-analyzed GPR data.

In Fig. 8(a) we show curves for measured attenuation lengths in ice [34] and the results reported here, using the longer estimated attenuation length at 150 MHz, from the ratio data. The attenuation length in ice is strongly temperature dependent. The temperature profiles in antarctic shelf ice and in glacial ice can vary significantly from site to site and often show an inversion at increasing depths. However, one can typically assume that a range of order 1 km of depth of ice with temperatures of $-20°$ to $-30°$C or colder can be found at most sites.

If we ignore for the moment the practical limits to contiguous volume of material, Fig. 8(b) shows the contained mass per volume with a radius of one attenuation length for ice and for the salt measurements we report here. It is evident that the significantly greater density of salt compared to ice (a factor of 2.4) leads to quite similar detection masses for salt and ice at $-30°$C. It is notable that in all cases the mass per attenuation volume exceeds 0.1 cubic km water equivalent for salt, and for ice below $-30°$C.

We note that the higher density of salt compared to ice, as well as the higher index of refraction, leads to several other differences in the behavior of Cherenkov emission from a

cascade within the medium. Cherenkov power W_c depends on the index of refraction n as

$$W_c \propto 1 - \frac{1}{n^2\beta^2} \tag{14}$$

where β is the particle velocity with respect to light speed. For ice at RF wavelengths, $n \simeq 1.6$, whereas for salt $n = 2.45$. Thus the Cherenkov output power is increased by 36% for $\beta = 1$, and there is an additional increase due to the fact that the Cherenkov threshold is $\sim 50\%$ lower than in ice, so particles of lower energy can contribute to the RF emission.

Because of the higher density, the cascade is also more compact by roughly the inverse of the density. Thus there is a decrease in the total tracklength of the shower and thus the Cherenkov power also decreases by roughly a factor of 2.4. For the same reason, however, the RF coherence of the shower is maintained to higher frequencies by roughly the same ratio and thus the coherent power output, which scales as $\nu^2\Delta\nu$ [11] will substantially offset the loss due to shorter tracklengths. Concerns over Fresnel effects would also be correspondingly reduced. [35]

A final note on RF propagation in ice concerns possible birefringence. Because of the complex crystal structure of ice, it is not surprising that both depolarization and rotation of the plane of polarization have been observed in both glacial and Antarctic ice [34]. At 440 MHz, the fractional difference in the index of refraction for the ordinary and extraordinary modes was found in some cases to exceed 5×10^{-4}, implying a rotation of the plane of polarization of $\Delta\Psi \simeq 0.45^\circ$ m^{-1}, about 3 times higher than the limit we measured for Hockley salt. (Recent gain calibration of the RICE detector may indicate less birefringence, however. [36]) Although measurements of polarization properties in salt are less complete, the lack of any evidence for strong birefringence, combined with the simple cubic lattice structure of the basic NaCl crystal leads to an expectation that salt may be superior to ice in this respect. Low birefringence could have importance for a cascade detection system since there is significant potential gain in event reconstruction if the polarization of the radio emission from the cascade can be made. [15]

VII. CONCLUSIONS

We have made initial measurements of the radio frequency attenuation lengths in natural halite in two underground salt excavations, the WIPP facility in New Mexico and the Hockley mine in Hockley salt dome in south Texas. We find that WIPP halite is quite lossy, due most likely to entrapped brine and other impurities, and is not suitable for a large scale detector for high energy neutrinos.

The salt in the Hockley mine is, by contrast, extremely transparent over the range from 150 to 750 MHz, with probable VHF and UHF attenuation lengths of several hundred meters or more. These long attenuation lengths are supported by several separate analyses: absolute field intensity, electric field measurements vs. distance, relative measurements vs. distance, and GPR data. The obtained values are especially long when one considers the density of salt relative to water. In addition, there is no apparent depolarization or significant scattering of the signals over a 45 m distance. The noise environment appears to be extremely quiet, consistent with a 310K black-body. Thus salt appears to provide a suitable medium for

potential neutrino detectors using embedded antennas in a manner similar to that of the RICE experiment in ice at the south pole.

To illustrate the potential power of a saltbed neutrino detector, we assume a $10 \times 10 \times 10$ antenna array on a 200 m grid spacing, with center frequency at 150 MHz and a 50% bandwidth, and a 300 m attenuation length at 300 MHz with a constant loss tangent with frequency as expected for salt. Such an array has an instrumented volume of about 8 km^3 and would easily fit within the top 3 km of a salt formation such as the Hockley dome. A Monte Carlo simulation of this array indicates that we would detect (4 antennas hit with a voltage SNR of 4 σ) of order 10 events per year from the minimal GZK neutrino flux [37] and up to 50 events per year if the flux is the maximum allowed value. For other models of high energy neutrino fluxes, we expect of order 5-10 events per year from gamma-ray bursts [38] depending on source evolution, and over 400 events per year from a representative AGN neutrino model [39]. The rate of such thermal coincidences over the course of a year is a few tens of events which would be easily removed by offline event reconstruction. The overburden of radio-absorbing rock protects the array from man-made radio-frequency interference.

Further work remains to be done to make more precise measurements of these remarkably long attenuation lengths, but the salt appears to present a viable medium for large calorimetric detectors in the mass range of 10-100 cubic kilometers of water-equivalent mass to detect cosmic neutrinos.

ACKNOWLEDGMENTS

We thank Roger Nelson, Norbert Rempe, Rey Carrasco, and other members of the WIPP staff for invaluable assistance with operations in the mine. We thank Dennis Bradley, Michael Nigh, and Alan Simon for their generous help in our Hockley mine measurements, and United Salt Corporation for their support of this endeavor. This work has been supported in part at UCLA by the U.S. Dept. of Energy, in particular its Advanced Detector Research Program, and by the National Science Foundation. This work has been performed in part at the Jet Propulsion Laboratory, California Institute of Technology, under contract with the National Aeronautics and Space Administration. The Stanford Linear Accelerator Center is supported by the U.S. Department of Energy, with work performed under contract DE-AC03-76SF00515.

---

[1] K. Greisen,"End to the Cosmic Ray Spectrum?," *Phys. Rev Lett.* **16**,748 (1966); G.T. Zatsepin and V. A. Kuz'min, *JETP Letters* **4**, 78 (1966).

[2] R. Engel, D. Seckel, & T. Stanev, "Neutrinos from propagation of ultra-high energy protons," astro-ph/0101216 and references therein provides a recent comprehensive summary of the GZK neutrino connection.

[3] C.T. Hill and D, N. Schramm, "Ultrahigh-energy cosmic-ray spectrum," *Phys. Rev. D***31**,564 (1985); F.W. Stecker, "Effect of Photomeson Production by the Universal Radiation Field on High-Energy Cosmic Rays," Phys. Rev. Lett. 21, 1016-1018 (1968).

[4] Amanda Collaboration, "Particle Astrophysics with the Amanda Neutrino Telescope," Annalen Phys. **10**, 131, 2001.
[5] Antares Collaboration, "A Deep Sea Telescope for High Energy Neutrinos," astro-ph/9907432.
[6] The Icecube NSF proposal, `http://pheno.physics.wisc.edu/icecube/`
[7] G. M. Frichter, J. P. Ralston, and D. W. McKay, Phys. Rev. D. **53**, 1684 (1996).
[8] D. Besson *et al.*, Proc. 26th. Intl. Cosmic Ray Conf., (1999).
[9] D. Besson *et al.*, Proc. RADHEP 2000, eds. D. Saltzberg & P. Gorham, Amer. Inst. of Phys., 2001.
[10] G. A. Askaryan, Zh. Eksp. Teor. Fiz. **41**, 616 (1961) [Soviet Physics JETP **14**, 441 (1962)]; G. A. Askaryan, Zh. Eksp. Teor. Fiz. **48**, 988 (1965) [Soviet Physics JETP **21**, 658 (1965)].
[11] E. Zas, F. Halzen, and T. Stanev, Phys. Rev. D **45**, 362 (1992).
[12] J. Alvarez–Muñiz and E. Zas, Phys. Lett. B, **411**, 218 (1997).
[13] J. Alvarez–Muñiz and E. Zas, Phys.Lett. B, **434**, 396, (1998).
[14] P. W. Gorham, D. P. Saltzberg, P. Schoessow, *et al.*, "Radio-frequency measurements of coherent transition and Cherenkov radiation: Implications for high-energy neutrino detection," Phys. Rev. E **62**, 8590, (2000).
[15] D. Saltzberg, P. Gorham, D. Walz, *et al.*, "Observation of the Askaryan Effect: Coherent Microwave Cherenkov Emission from Charge Asymmetry in High Energy Particle Cascades," Phys. Rev. Lett. **86**, 2802, (2001).
[16] See the Proc. RADHEP 2000, eds. D. Saltzberg & P. Gorham, Amer. Inst. of Phys., 2001.
[17] M. Chiba, et al., "Study of Salt Neutrino Detector," Proc. RADHEP 2000, Amer. Inst. of Phys., 2001.
[18] M. A. Hanna, "Geology of Gulf coast salt domes," in *Problems of Petroleum Geology, A symposium*, eds. W. Wrather & F. Lahee, T. Murphy & Co. London, (1934).
[19] M. T. Halbouty, *Salt Domes: Gulf Region, United States & Mexico*, Gulf publishing Co., Houston, TX (1967).
[20] R. G. Breckenridge, "Low Frequency dispersion in ionic crystals," Journ. Chem. Phys. 16 (10), 959, (1948).
[21] A. von Hippel, *Dieletric materials and applications*, Wiley and Sons, New York, 1954.
[22] A. P. Annan, J. L. Davis, D. Gendzwill, "Radar sounding in potash mines, Saskatchewan, Canada," Geophysics **53**, 1556 (1988).
[23] R. R. Unterberger, "Radar propagation in rock salt," Geophys. Prospecting **26**, 312, (1978).
[24] R. D. Stewart & R. R. Unterberger, "Seeing through rock salt with radar," Geophysics **41**, 123, (1976).
[25] S. J. LeFond, *Handbook of World Salt Resources*, Plenum press, New York, (1969).
[26] G. R. Olhoeft, "Electrical Properties of salt cored from Carlsbad, New Mexico," U.S. Geological Survey Open File Report 78-463, (1978).
[27] M. Kannenberg & W. M. Roggenthen, Env. and Eng. Geosci. **3**, 349, (1997).
[28] W. M. Roggenthen, personal comm. (2000).
[29] R. R. Unterberger, Holser and Brown, Geophysics **35**, 1149 (1970).
[30] J. A. Hluchanek, "Radar investigations of the Hockley salt dome," unpublished Master's thesis, Texas A&M univ., (1973).
[31] C. H. Ritz, Bull. AAPG 20, 1413, (1936).
[32] J. Kraus, *Antennas*, 2nd edition, McGraw-Hill, Boston, MA (1988).
[33] W. T. Holser, *et al.*., "Radar logging of a salt dome," Geophysics **37**, 889, (1972).

[34] V. V. Bogorodsky, C. R. Bentley, & P. E. Gudmandsen, *Radioglaciology*, D. Reidel, Dordrecht, translated from Russian, (1985).

[35] R. Buniy and J. Ralston, "Radio Detection of High-Energy Particles: Coherence vs. Multiple Scales", astro-ph/0003408; R. Buniy and J. Ralson, "Concepts in the Coherence of Radio Cherenkov Emission from Ultra-High Energy Electromagnetic and Hadronic Showers," in Proc. RADHEP 2000, eds. D. Saltzberg & P. Gorham, Amer. Inst. of Phys., 2001.

[36] D. Seckel *et al.* (RICE Collaboration), "Radiofrequency Properties of Antarctic Ice and Calibration of the RICE Detector", in Proc. of the 27th Intl. Cosmic Ray Conference, Hamburg, Germany (2001).

[37] R. Engel, D. Seckel, T. Stanev, Phys. Rev. **D64** 093010 (2001).

[38] E. Waxman and J. Bahcall, Astrophys. J. **541**, 707 (2000).

[39] K. Mannheim, Astroparticle Physics **3**, 295 (1995).